MRS Advances © 2019 Materials Research Society DOI: 10.1557/adv.2019.342



A Review of Advances in Thermophotovoltaics for Power Generation and Waste Heat Harvesting

Abigail Licht, Nicole Pfiester, Dante DeMeo, John Chivers, and Thomas E. Vandervelde

The Renewable Energy and Applied Photonics Laboratories, Electrical and Computer Engineering Department, Tufts University, Medford, MA 02155 USA

ABSTRACT

The vast majority of power generation in the United States today is produced through the same processes as it was in the late-1800s: heat is applied to water to generate steam, which turns a turbine, which turns a generator, generating electrical power. Researchers today are developing solid-state power generation processes that are more befitting the 21st-century. Thermophotovoltaic (TPV) cells directly convert radiated thermal energy into electrical power, through a process similar to how traditional photovoltaics work. These TPV generators, however, include additional system components that solar cells do not incorporate. These components, selective-emitters and filters, shape the way the radiated heat is transferred into the TPV cell for conversion and are critical for its efficiency. Here, we present a review of work performed to improve the components in these systems. These improvements will help enable TPV generators to be used with nearly any thermal source for both primary power generation and waste heat harvesting.

Introduction

Thermophotovoltaics (TPVs) convert infrared radiation, or heat, into electricity. TPVs have a wide-range of applications due to the fact that they can be paired with any heat source. Applications include, for example, converting heat from combustion in a microscale battery [1]-[7], from radioisotopes for deep-space power generation [8], [9], and from high-temperature industrial processes for recovering waste-heat [10].

A TPV system consists of three main components: a heat source, an emitter, and a TPV diode, Figure 1. The heat source is typically between 1,000K and 2,000 K. The emitter, which acts as an intermediate stage between the heat source and the TPV diode, allows for shaping of the radiant spectrum. The emitter can either be a blackbody that emits across all wavelengths, or a selective-emitter designed to radiate a narrow band of wavelengths matched to the TPV diode. In addition to spectral shaping at the emitter stage, the spectrum may be further refined through filtering prior to the diode stage, Figure 1.

The core of a TPV system is the photovoltaic diode; it is the component responsible for converting the incident radiation into usable power. The TPV diode generates a current and a voltage via the photovoltaic effect. Specifically, if the incident light contains photons with energy greater than the bandgap of the diode material, electrons may be excited from the valance band to the conduction band, where they can generate a current due to the built-in voltage of the TPV diode. The current and voltage are then delivered to the electrical load. TPV diodes typically have a current of approximately 1-3 A/cm² and a voltage of approximately 0.5 V for a power density of ~ 1 W/cm². This means that a 10x10 cm² array of cells can easily be used to generate 100+ Watts of power. Thus far, TPV systems have demonstrated efficiencies as high as ~20% [11]. Modelling indicates, however, that TPV system efficiencies could be as high as 40% [12], [13].



Figure 1. TPV system. Thermal energy from a heat source is absorbed by an emitter, which radiates infrared photons toward the TPV diode. Prior to the TPV diode stage, additional filtering may be incorporated. The radiation is then absorbed by the TPV diode, which generates a current and a voltage via the photovoltaic effect.

We will start with discussing the issue of extending the cut-off wavelength of TPV diodes. This is a critical element when attempting to harvest energy from lower temperature heat sources. We will follow with a review of the materials and growth techniques used in TPV diodes as these largely determine the cut-off wavelength. We will continue with a discussion the diode design and the benefits of introducing an intrinsic layer. This review will finish with new developments in front-surface contacts incorporating photonic crystals and ensuring that the contacts are of an ohmic nature. Extending the cut-off wavelength of TPV diodes

At present, TPV diodes are matched to only very high temperature heat sources. This limitation is primarily due to the bandgap of the TPV diode material. As stated previously, only photons with energy greater than the bandgap value may contribute to a photogenerated current within the diode. Since energy is inversely proportional to wavelength, TPV diodes cannot absorb radiation beyond a cut-off wavelength determined by the bandgap value.

The cut-off wavelengths of typical TPV diode materials are marked in Figure 2, along with spectra radiated from various temperature sources, approximated as

blackbody spectra. For a given temperature source, such as 1,000 K, we see that much of the spectrum is not being absorbed since it is beyond the cut-off wavelength. A reducedbandgap diode with a longer cut-off wavelength would allow for more of the spectrum to be absorbed. Moreover, a narrow bandgap diode could also be paired with lower temperature sources, enabling a new class of TPV applications. For example, TPVs could be used to absorb heat from car-exhaust.

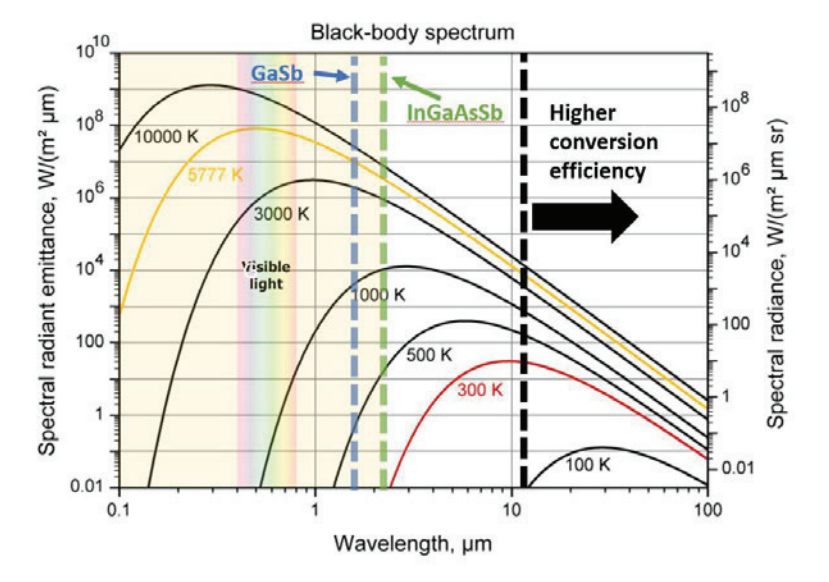


Figure 2. Blackbody spectrum for various temperatures. The cut-off wavelengths of two of the most common TPV diode materials, gallium antimonide (GaSb) and quarternary alloy indium gallium arsenide antimonide InGaAsSb, are marked by the leftmost (blue) and middle (green) dashed lines at 1.7 and 2.3 μm , respectively. If the cut-off wavelength could be extended to longer wavelengths e.g. the rightmost (black) dashed line, the diode would be able to absorb more of the incident spectrum, yielding a higher short circuit current which can lead to higher efficiencies. A longer cut-off wavelength diode could also be used to absorb radiation from lower temperature sources, enabling new applications for TPVs. Figure is adapted from Sun.org and reproduced with permission under the Creative Commons 4.0 agreement [14].

Much of the progress in TPVs has stemmed from developments in the field of photovoltaics. The first implementation of TPV was in the mid-1950's when Henry Kolm of MIT Lincoln Laboratory held a silicon solar cell up to a lantern in an attempt to generate electricity from a flame [15]-[18], making silicon the first diode material used in TPVs. Silicon, however, has a bandgap of 1.12 eV and cut-off wavelength ~1.1 µm. This wavelength is well matched to the blackbody spectrum of the sun and is thus nearly ideal for solar applications, however, it is poorly matched to TPV applications with lower source temperatures of ~ 1,000-2,000 K. In order to employ silicon in TPV applications, silicon must be paired with selective emitters such as ytterbia, Yb2O3, to tailor the spectrum to the silicon diode [19], [20].

Germanium, a common bottom cell material from multi-junction solar cells, has also been investigated as a possibility for TPV diodes [21]. Germanium is a better match for

TPV applications than silicon, since germanium has a lower bandgap 0.66eV and absorbs wavelengths out to 1.88 µm [20]. However, germanium is still an indirect bandgap material and has generally poor performance. Recent research has focused mostly on III-V semiconductors which are direct bandgap materials with a wider range of potential bandgaps with which to design TPV diodes.

III-Vs and their alloys

With the exception of the group IV materials discussed previously, the majority of TPV diodes consist of III-V materials, which contains atoms from group III and V of the periodic table, Figure 3. Materials used include binaries such as InAs and GaSb and their alloy derivatives. While binaries are easier to produce, alloys allow for more possibilities since in theory they can be used to create any bandgap value within the range of the binary values, Figure 4. In practice, however, the alloys that can be used are often limited to the composition that is lattice-matched to the available substrates, which include: InAs, InP, and GaSb. Lattice matching is crucial because if the material and substrate are not matched, defects may occur during the growth of the material that will decrease the performance of the TPV diode.



 $Figure \ 3. \ Excerpt \ from \ the \ periodic \ table \ highlighting \ the \ group \ III \ and \ V \ elements \ that \ are \ incorporated \ into \ TPV \ diode$ materials

The leading materials that have been researched in the past few decades have been InGaAsSb and GaSb on a GaSb substrate and InGaAs and InAsP on an InP substrate. Binary GaSb is the most frequently used TPV material, with a bandgap value of 0.72 eV at 300K. GaSb was originally developed for multi-junction solar cells [23]. GaSb has a direct bandgap and therefore a relatively high efficiency. GaSb is the only diode material to be incorporated into a commercial TPV application thus far [24]. InGaAsSb, also referred to as GaInAsSb, is another antimonide compound that has been actively researched. It has a bandgap ~0.5eV when it is grown lattice matched to GaSb [25].

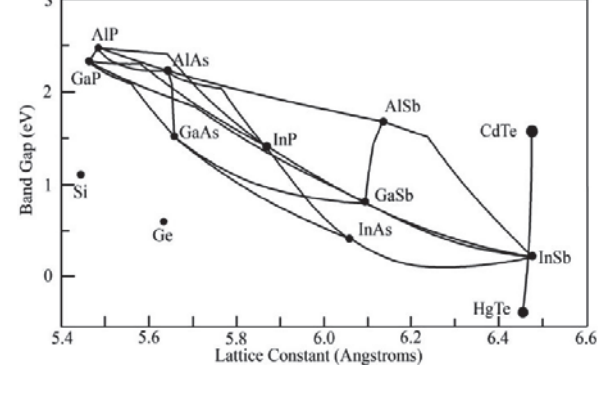


Figure 4. Bandgap versus lattice parameter for various materials. Lines between materials show the bandgap for the various alloys. With the current technology we are limited to alloy compositions lattice-matched to the available substrate materials, such as InP, InAs, and GaSb. Figure is reproduced with permission under the Creative Commons 3.0 agreement from the journal Sensors [22].

InGaAs can be grown lattice matched to InP with $E_{\rm g}$ =0.74 eV, or mismatched in the range of ~0.5-0.6 eV. The lowest bandgap achieved thus far for InGaAs has been 0.52 eV [26]. InGaAsP/InP has also been researched as a TPV diode material. A major advantage of using this quaternary alloy over the ternary InGaAs is that quaternary alloy has two degrees of freedom and, therefore, there is a wider range of bandgap values that can be obtained while maintaining lattice matching to the substrate. The addition of phosphorous allows for extension to longer wavelength, lower bandgap diodes, in the range of 0.3-0.55 eV. As with most narrow bandgap diodes, however, increased Auger recombination becomes a major issue. Another phosphorous alloy, InAsSbP, has been grown lattice matched to InAs [27]-[29], and has a similar bandgap range to that of InGaAsP/InP. Lastly, InAs has also been recently investigated for TPVs. This is the lowest bandgap bulk material investigated for TPVs thus far; with a bandgap of 0.32eV, InAs covers wavelengths out to 3.9 μ m [30].

A sampling of the performance of various TPV diode materials is tabulated in Table 1. From this table we note that the present technology covers a range from 0.74 eV down to $\sim\!0.3$ eV. A direct comparison between the materials is not necessarily fair, given that they are characterized under a wide range of testing conditions. For example, the short-circuit current in a diode will be larger when using an illumination source of higher intensity. Therefore, a perhaps better method of comparison is the quantum efficiency, which shows how well each diode absorbs at a given wavelength, irrespective of the light source. The quantum efficiency of several common diode materials is plotted in Reference [31]. The data shows that GaSb and InGaAsSb have demonstrated the best QEs thus far. This is an area of active research though and some new possibilities are on the horizon [31]–[35]. Voltage factor is defined as the ratio of the open circuit voltage to the bandgap of the material $qV_{\rm OC}/E_{\rm G}$.

Table 1. Table of TPV diode performance for various materials. The bandgap (E_G) , cut-off wavelength (λ_C) , short circuit current (J_{SC}), open-circuit voltage (V_{OC}), fill factor (FF), and voltage factor (V_F) are reported.

Material	$E_{G}(eV)$	λ_{C} (μ m)	$J_{SC} (A/cm^2)$	$V_{OC}(V)$	FF	V_{F}	REF
InGa _{0.53} As _{0.47}	0.74	1.7	1	0.47	0.64	0.63	[36]
GaSb	0.72	1.7	3	0.41	-	0.57	[37]
InGa _{0.69} As _{0.31}	0.60	2.1	2.26	0.36	0.67	0.59	[38]
InGaSb	0.56	2.2	3	0.27	-	0.48	[39]
InGaAsSb	0.53	2.4	1	0.30	-	0.57	[40]
InAsSbP	0.35	3.5	3	0.12	-	0.34	[41]
GaInAsPSb	0.34	3.6	0.29	0.03	0.33	0.08	[42]
InAs	0.32	3.9	0.89	0.06	0.37	0.19	[30]

III-V Growth Techniques

Techniques used to grow III-V materials include metal-organic chemical vapor deposition (MOCVD), liquid phase epitaxy (LPE), and molecular beam epitaxy (MBE). Of these methods, MBE is best suited for antimonide and more complex material growth (e.g. superlattices, quantum dots, etc.) [43], [44], [53], [45]-[52]. MOCVD has proven difficult for antimonide growth due to the lack of precursor materials for the antimonides and the higher growth rates and temperatures required. Moreover, bulk techniques like LPE lack the control necessary to accurately grow layers with sharp transitions as required for some structures such as superlattices, which can be grown much more easily with MBE. The thickness of each layer in MBE growth can be precisely controlled with appropriate shuttering of the source materials, and the ultra-high vacuum allows for highpurity material growth.

GaSb pin diodes

Doping in GaSb TPV diode structures is often achieved via diffusion methods. This method limits the design since the doping profile is fixed to the gradient formed by diffusion. An alternative method is to fabricate the diode structure epitaxially. This method allows for a sharply defined junction and the formation of more advanced architectures such as those that include back surface fields and front surface windows. The epitaxial method also uniquely allows for the introduction of an intrinsic region between the P and N regions. Adding an intrinsic region is a technique employed in various PV technologies to extend the electric field within the device, increasing collection of photogenerated carriers. This method could improve carrier collection in GaSb diodes with photonic crystals (PhCs), where the shifted absorption profile due to the PhCs extends well into the device.

The intrinsic carrier concentration for GaSb at room temperature is calculated to be 1.5 ×10¹²/cm³ [54]-[57]. In practice, however, the carrier concentration is much higher -10¹⁶ - 10¹⁷/cm³ - due to native defects [55]. These defects arise from the low vapor pressure and surface mobility of antimony, which causes antimony atoms to cluster together, leaving anti-sites where antimony atoms would normally incorporate into the lattice [58]. The anti-site is unstable and the nearest gallium atom will fill the site, creating both a gallium-in-antimony site defect ("Gasb") and a gallium vacancy defect ("V_{Ga"}). These defects limit the intrinsic carrier concentration in practice to a value much higher than the theoretical value.

The addition of an intrinsic layer in a GaSb diode was investigated by Licht et. al. [59] through computer simulations, with experimental results pending at the time of this publication. The structure consisted of an 80nm n-type top layer, 1.0μm n.i.d. intrinsic region, 2.8μm p-type GaSb base layer, and a 100nm AlSb back side field (BSF) layer, as depicted in Figure 5. The BSF layer is a highly doped, wide-bandgap region that creates a potential barrier for minority carrier electrons. This serves to reflect the electrons back towards the electric field of the pin junction thus reducing parasitic rear-surface recombination. The device structure used an n-on-p architecture because the minority carrier electrons in a p-type absorber have a much greater mobility than the minority carrier holes in an n-type absorber. The intrinsic region was made thick enough to extend the space charge region yet not too thick as to cause the electric field drop too low due to increased series resistance to shuttle the carriers towards the contacts. These simulations indicate an expected improvement of 6% in efficiency and an increase of 10% in internal quantity efficiency at a wavelength of 1.3μm relative to a pn control diode.



Figure 5. Simulated pin GaSb structure as described in [59]. The addition of the intrinsic region as compared to a pn structure expands the space charge region and related electric field, thus increasing the amount of photogenerated carriers

Considering these results, avenues to further decrease the background concentration in GaSb are worthy of investigation. Several methods have already been explored [58], [60]. In one technique, the GaSb epilayer is grown on tilted substrates to encourage Sbincorporation; this method has demonstrated background carrier concentrations on the order of $10^{15}/\mathrm{cm}^3$ [58]. In another technique, Polyakov *et al.* achieved a low doping on the order of $10^{13}/\mathrm{cm}^3$ by growing GaSb at higher temperatures than normal - 600-630°C as opposed to 500°C [60]. Given these promising results, the lower predicted background doping concentrations of $\sim 10^{12}/\mathrm{cm}^3$ could be attainable. Inclusion of an intrinsic layer would be of benefit to other materials [61] including other III-V diodes, as such similar studies comparing pn to pin structures should be studied for these materials as well

GaSb Diodes with Front-Surface Photonic Crystals

In addition to extending TPV diodes to longer wavelengths, additional mechanisms can be employed to improve upon the existing TPV diode technologies. One method researched to improve the efficiency of GaSb TPV diodes is through the incorporation of front-surface two-dimensional metallic photonic crystals (MPhCs), Figure 6. MPhCs can be fabricated directly onto the diode aperture using standard metallization and lithography techniques, where they can be used to strategically alter the absorption in the GaSb diode. These repeating nanoscale structures create a photonic bandgap, allowing certain wavelengths of light to pass through while blocking others. This structure can be used to block out undesirable wavelengths, allowing for transmission of only near-bandgap radiation. In addition to filtering, the MPhCs can also be used to strategically

alter the photo-absorption profile within the device structure. The non-infinite height of the MPhC pattern causes the evanescent field to "leak" into the semiconductor material. This allows for absorption at a greater depth in the device structure than traditional alldielectric anti-reflective coatings. Absorption deeper into the device can be advantageous, as GaSb suffers from parasitic recombination at the front-surface.

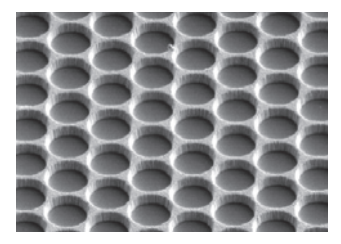


Figure 6. SEM image of metallic photonic crystals deposited onto GaSb

MPhCs were first proposed for spectral engineering in GaSb TPV diodes in 2012 [62]. Initial work by Shemelya et. al. demonstrated an increase in the absorption through the incorporation of 2D MPhCs [63], [64]. This improvement in the absorption led to an increase in the photogenerated current [63]. However, these MPhCs were deposited onto GaSb diodes that were poor-performing, as can be seen by the low measured open-circuit voltage values, which translate to voltage factors of only ~0.2. Table 2 shows the results from Shemelya et.al. with three different front-surface layers, including a standard antireflective coating (ARC).

Table 2. Open-circuit voltage and voltage factors for GaSb diode with and without PhCs.

	$V_{OC}(mV)$	V_{F}
SiN & ARC	175	0.241
PhC - No ARC	142	0.196
PhC & ARC	165	0.227

Ohmic contact/PhC layer

Photonic crystals incorporated onto the front surface of the GaSb TPV diodes not only to improve the absorption in the device, but also act as a front contact. The contacts used by Shemelya et. al. [63] consisted of a material composition of titanium, platinum, and gold to both p-GaSb and n-GaSb [65]. However, this material composition does not readily form an ohmic contact to n-GaSb. Here, we discuss why this is the case and consider alternative options.

When a semiconductor and metal are brought into contact under equilibrium, the Fermi levels will align. For some semiconductor materials, including GaSb, the Fermi level is fixed at the surface independent of the metal it mates to and is therefore "pinned" [66]. In GaSb, the Fermi level is pinned near the valence band at the surface [55], [66]-[68]. While pinning near the valence band facilitates contact to p-GaSb, it makes contact to n-GaSb extremely difficult. Upon alignment of the Fermi levels for a metal and n-GaSb, a large barrier will form, blocking carrier transport from the semiconductor to the metal. One method to overcome the barrier is to highly dope the material; high doping thins the depletion region at the metal-semiconductor interface so that carriers can tunnel through the barrier. As mentioned previously, however, highly doped n-GaSb is difficult to achieve due to the intrinsic p-type defects in GaSb.

Because of the technological importance of antimonides, a significant amount of research has focused on developing ohmic contacts to n-GaSb [69], [70], [79], [80], [71]-[78]. Originally gold-based contact recipes were researched [72]-[75], [77]. Gold-based contacts are not recommended for GaSb as the gold diffuses deep into the device [80]. Palladium-based contact recipes have been quite successful, with resistivity as low as ~10-6 Ω-cm² with annealing [76]-[79]. These Pd-based contacts are usually combined with another material like germanium to create a heavily doped layer beneath the contact. The contact recipes are then composed of several layers. For example one successful recipe consisted of Pd/Ge/Au/Pt/Au [77], where first gold layer is to encourage diffusion of Ge into semiconductor. One concern with this method, however, is that the deposited contacts must be annealed in order to form an ohmic contact. Heating the devices can be troublesome as it may lead to further out-diffusion of antimony and degradation of the device structure. Another concern unique to our design is that the n-type contact material must also serve as the material for the PhC pattern. The effect of using these multi-layer stacks for PhCs would have to be studied via finite-difference time-domain simulations.

Rather than incorporating multi-layer metal compositions for the PhCs, an alternative solution is to introduce a contact layer (CL). The CL would be a thin layer of a material for which the Fermi level is pinned in a more ideal location. When inserted just beneath the contact, the CL facilitates formation of an ohmic contact to the top layer of the diode. This technique has been employed with other III-V materials; for example, InAs is frequently used as a CL with III-V materials because the surface Fermi level of InAs is pinned above the conduction band, allowing for a low contact resistance. InAs cannot be used as a contact layer for GaSb diodes because of the band discontinuity between InAs and GaSb. This band alignment issue can be circumvented, however, if InAs is alloyed with Sb [81]-[83]. The alloy InAsSb is a good candidate for a CL for n-type GaSb as the Fermi level is pinned in the conduction band and the alloy can be highly doped. InAsSb lattice matched to GaSb has been explored as a CL, achieving specific resistivity as low as 5.1 x $10^{-6} \Omega$ -cm² without annealing [82]. The quaternary alloy GaInAsSb has also been researched as a CL for GaSb: Huang *et al.* achieved a contact resistivity of $2 \times 10^{-6} \Omega$ -cm² by using GaInAsSb as a contact layer [83].

It appears the best solution to create an ohmic contact to n-GaSb for an n-on-p GaSb diode might be to incorporate a contact layer. A major advantage of using a CL is that it does not require annealing to achieve a low resistivity. Also, by using a CL, less complicated contact/PhC recipes are inherently possible.

Conclusion

While thermophotovoltaics (TPVs) have the potential to be applied with near ubiquity to harvest energy from any heat source, in practice the technology is not yet available for practical sources with temperatures below a few hundred Celsius. As discussed in References [84], [85], there has been a recent explosion in research into selective emitters based around the advances in frequency-selective surfaces. Here, we focused on the significant advances which have been made in diode design and filter technology. Numerous new materials are on the horizon for TPVs, building off of the foundational work in III-Vs and Group-IV materials, with Bi- or Tl-compounds and Sn-compounds, respectively. We have entered a new era of advancement of TPV

components with great advances coming out, bringing us closer to the realizing the promise of this technology, which could change the global energy landscape.

```
References
<sup>1</sup> L.M. Fraas and J. Strauch, in TPV-9 (Valencia Spain, 2010), pp. 2-7.
<sup>2</sup> B. Bernd, D. Wilhelm, and H. Reto, Appl. Energy 105, 430 (2013).
<sup>3</sup> W.M. Yang, S.K. Chou, and J. Li, Appl. Therm. Eng. 29, 3144 (2009).
<sup>4</sup> S.K. Chou, W.M. Yang, K.J. Chua, J. Li, and K.L. Zhang, 88, 1 (2011).
<sup>5</sup> W.M. Yang, S.K. Chou, C. Shu, Z.W. Li, and H. Xue, Appl. Phys. Lett. 84, 3864 (2004).
<sup>6</sup> W.E. Horne, M.D. Morgan, V.S. Sundaram, and T. Butcher, AIP Conf. Proc. 653, 91 (2003).
O.M. Nielsen, L.R. Arana, C.D. Baertsch, K.F. Jensen, and M. a. Schmidt, TRANSDUCERS '03. 12th
Int. Conf. Solid-State Sensors, Actuators Microsystems. Dig. Tech. Pap. (Cat. No.03TH8664) 1, 714
  A. Schock, M. Mukunda, C. Or, and G. Summers, Acta Astronaut. 37, 21 (1995).
<sup>9</sup> V.L. Teofilo, P. Choong, J. Chang, Y.-L. Tseng, and S. Ermer, J. Phys. Chem. C 112, 7841 (2008).
<sup>10</sup> A. Thekdi and S.U. Nimbalkar, (2015).
11 B. Wernsman, R.R. Siergiej, S.D. Link, R.G. Mahorter, M.N. Palmisiano, R.J. Wehrer, R.W. Schultz,
G.P. Schmuck, R.L. Messham, S. Murray, C.S. Murray, F. Newman, D. Taylor, D.M. DePoy, and T.
Rahmlow, Greater than 20% Radiant Heat Conversion Efficiency of a Thermophotovoltaic
Radiator/Module System Using Reflective Spectral Control (2004), pp. 512–515.
 <sup>2</sup> E. Kittl, in 10th IEEE Photovolt. Spec. Conf. (1974), pp. 103–106.
<sup>13</sup> A. Datas, Sol. Energy Mater. Sol. Cells 134, 275 (2015).
<sup>14</sup>(n.d.).
15 J.Y. Wah, PhD Thesis, University of Essex, 2003.
16 M.W. Dashiell, J.F. Beausang, H. Ehsani, G.J. Nichols, D.M. Depoy, L.R. Danielson, P. Talamo, K.D.
Rahner, E.J. Brown, S.R. Burger, P.M. Fourspring, W.F. Topper Jr., P.F. Baldasaro, C.A. Wang, R.K.
Huang, M.K. Connors, G.W. Turner, Z.A. Shellenbarger, G. Taylor, J. Li, R. Martinelli, D. Donetski, S.
Anikeev, G.L. Belenky, and S. Lurvi, IEEE Trans. Electron Devices 53, 2879 (2006).
  H. Mohseni, V.I. Litvinov, and M. Razeghi, Phys. Rev. B (Condensed Matter) 58, (1998).
<sup>18</sup> H. Kolm, Solar-Battery Power Source Quarterly Progress Report Solid State Research, Group 35
(Lexington, MA: MIT Lincoln Laboratory, 1956).

19 B. Bitnar, Semicond Sci Technol 18, 221 (2003).
<sup>20</sup> T. Bauer, Thermophotovoltaics: Basic Principles and Critical Aspects of System Design (Springer,
<sup>21</sup> M.A. Green, K. Emery, Y. Hishikawa, W. Warta, and E.D. Dunlop, Prog. Photovoltaics Res. Appl. 20,
12 (2012).
  C. Downs and T.E. Vandervelde, Progress in Infrared Photodetectors since 2000 (2013).
<sup>23</sup> Lewis Fraas, J. Avery, J. Gee, and K. Emery, in IEEE PV Spec. Conf. (1990), p. 190.
<sup>24</sup> L.M. Fraas, H.X. Huang, S.Z. Ye, S. Hui, A. J, and B. R, in 3rd REL Conf. Thermophotovoltaic Gener.
Electr. (1997), pp. 33-40.
  a. P. Astakhova, B.E. Zhurtanov, a. N. Imenkov, M.P. Mikhailova, M. a. Sipovskaya, N.D. Stoyanov,
and Y.P. Yakovlev, Tech. Phys. Lett. 33, 11 (2007).
<sup>26</sup> R.J. Wehrer, AIP Conf. Proc. 738, 445 (2004).
<sup>27</sup> E.V. Kunitsyna, I. a. Andreev, V.V. Sherstnev, T.V. L'vova, M.P. Mikhailova, Y.P. Yakovlev, M.
```

- Ahmetoglu (Afrailov), G. Kaynak, and O. Gurler, Opt. Mater. (Amst). **32**, 1573 (2010).

 ²⁸ V.A. Gevorkyan, V.M. Aroutiounian, K.M. Gambaryan, A.H. Arakelyan, I. a. Andreev, L. V. Golubev,
- Y.P. Yakovlev, and M.W. Wanlass, AIP Conf. Proc. 890, 165 (2007).
- ²⁹ M. V Andreev, O.A. Khvostikov, V P Khvostikova, and E. V Oliva, in *Thermophotovoltaic Gener*. Electr. 5th Conf. Thermophotovoltaic Gener. Electr. (AIP Conf. Proc. 653) (2003), p. pp 383-91.
- A. Krier, M. Yin, M.R. J., and S.E. Krier, J. Electron. Mater. 45, 2726 (2016).
- ³¹ M. Mauk, Mid-Infrared Semicond. Optoelectron. **118**, 673 (2006).
- ³² M. Stevens, A. Licht, N. Pfiester, E. Carlson, K. Grossklaus, and T.E. Vandervelde, 2017 IEEE 44th Photovolt. Spec. Conf. (2017)
- A. Zayan, M. Stevens, and T.E. Vandervelde, Conf. Rec. IEEE Photovolt. Spec. Conf. ember, 2839 (2016).
- A. Zayan, C. Downs, and T.E. Vandervelde, 29th Eur. Photovolt. Sol. Energy Conf. Exhib. (EU PVSEC 2014) (2015).
- ⁵ C. Downs and T.E. Vandervelde, Conf. Rec. IEEE Photovolt. Spec. Conf. 000462 (2011).

(1997).

³⁹ P.S. Dutta, J.M. Borrego, H. Ehsani, G. Rajagopalan, I.B. Bhat, R.J. Gutmann, G. Nichols, and P.F. Baldasaro, AIP Conf. Proc. 653, 392 (2003). ⁰ H.K. Choi, C.A. Wang, G.W. Turner, M.J. Manfra, D.L. Spears, G.W. Charache, L.R. Danielson, H.K. Choi, C.A. Wang, G.W. Turner, M.J. Manfra, and D.L. Spears, 3758, 1 (2003). M.G. Mauk, O. V Sulima, J.A. Cox, and R.L. Mueller, in 3rd World Conf. Photovolloic Energy Convers. (2003), pp. 224-227. K.J. Cheetham, P.J. Carrington, N.B. Cook, and A. Krier, Sol. Energy Mater. Sol. Cells 95, 534 (2011). ⁴³ D. Demeo, C. Shemelya, C. Downs, A. Licht, E.S. Magden, T. Rotter, C. Dhital, S. Wilson, G. Balakrishnan, and T.E. Vandervelde, J. Electron. Mater. 43, 902 (2014). 44 R. Rehm, M. Masur, J. Schmitz, V. Daumer, J. Niemasz, T. Vandervelde, D. DeMeo, W. Luppold, M. Wauro, A. Wörl, F. Rutz, R. Scheibner, J. Ziegler, and M. Walther, Infrared Phys. Technol. 59, 6 (2013). ⁴⁵ J. Shao, T.E. Vandervelde, A. Barve, W.-Y. Jang, A. Stintz, and S. Krishna, J. Vac. Sci. Technol. BNanotechnology Microelectron. 29, (2011). ⁴⁶ J. Shao, T.E. Vandervelde, A. Barve, A. Stintz, and S. Krishna, Appl. Phys. Lett. 101, (2012). ⁴⁷ J.R. Andrews, S.R. Restaino, S.W. Teare, Y.D. Sharma, W.-Y. Jang, T.E. Vandervelde, J.S. Brown, A. Reisinger, M. Sundaram, S. Krishna, and L. Lester, IEEE Trans. Electron Devices 58, 2022 (2011). ⁴⁸ P. Vines, C.H. Tan, J.P.R. David, R.S. Attaluri, T.E. Vandervelde, and S. Krishna, IEEE J. Quantum Electron. 47, 607 (2011). A.V. Barve, Y.D. Sharma, J. Montoya, J. Shao, T. Vandervelde, T. Rotter, and S. Krishna, Int. J. High Speed Electron. Syst. 20, 549 (2011). A. Barve, J. Shao, Y.D. Sharma, T.E. Vandervelde, K. Sankalp, S.J. Lee, S.K. Noh, and S. Krishna, IEEE J. Quantum Electron. 46, 1105 (2010). T.E. Vandervelde and S. Krishna, J. Nanosci. Nanotechnol. 10, 1450 (2010). 52 T.E. Vandervelde, K. Sun, J.L. Merz, A. Kubis, R. Hull, T.L. Pernell, and J.C. Bean, J. Appl. Phys. 99, (2006). ³ A.J. Kubis, T.E. Vandervelde, J.C. Bean, D.N. Dunn, and R. Hull, Mater. Res. Soc. Symp. Proc. 818, 411 (2004). G. Stollwerck, O. V Sulima, and A.W. Bett, 47, 448 (2000). 55 P.S. Dutta and H.L.B. Kumar, J. Appl. Phys. 81, 5821 (1997). ⁵⁶ I.P.-T. Institute, (n.d.). ⁵⁷ O. V Sulima and A.W. Bett, **66**, (2001). K.F. Longenbach, W.I. Wang, K.F. Longenbach, and W.I. Wang, 59, (1991).
 A.S. Licht, C. Shemelya, D.F. DeMeo, E.S. Carlson, and T.E. Vandervelde, in 2017 IEEE 60th Int. Midwest Symp. Circuits Syst. (IEEE, 2017), pp. 843–846. A.Y. Polyakov, M. Stam, A.G.M.G. Wilsonz, Q.F. Rai, R.J. Hillard, and A.Y. Polyakov, 1316, (1992). ⁶¹ M. Augustin, T. Markvart, and L. Castaner, *Practical Handbook of Photovoltaics*, 2nd Editio (Elsevier, 2012). 62 C. Shemeya and T.E. Vandervelde, J. Electron. Mater. 41, 928 (2012). ⁶³ C. Shemelya, D.F. Demeo, and T.E. Vandervelde, Appl. Phys. Lett. **104**, (2014). ⁶⁴ C.M. Shemelya, ProQuest Diss. Theses Glob. (2013). 65 D.F. Demeo, N.A. Pfeister, C.M. Shemelya, and T. Vandervelde, Proc. SPIE - Int. Soc. Opt. Eng. 8982, 66 K.M. Schirm, P. Soukiassian, P.S. Mangat, and L. Soonckindt, Phys. Rev. B 49, 5490 (1994). 67 W.E. Spicer, I. Lindau, P. Skeath, C.Y. Su, and P. Chye, Phys. Rev. Lett. 44, (1980). 68 Z.M. Lu, D. Mao, L. Soonckindt, and A. Kahn, J. Vac. Sci. Technol. A 8, 1988 (1990). 69 N. Rahimi, A.A. Aragon, O.S. Romero, D.M. Shima, T.J. Rotter, D. Sayan, G.B.F. Lester, N. Rahimi, A.A. Aragon, O.S. Romero, D.M. Shima, T.J. Rotter, S.D. Mukherjee, G. Balakrishnan, and L.F. Lester, 108, 1 (2014). ⁷⁰ J.A. Robinson and S.E. Mohney, Solid. State. Electron. 48, 1667 (2004). ⁷¹ A. Subekti, V.W.L. Chin, T.L. Tansley, and I.I. June, **39**, 329 (1996). ⁷² C. Heinz, Int. J. Electron. **54**, 247 (1983). 73 X. Li and A.G. Milnes, **143**, 1014 (1996). ⁷⁴ M. Rolland, S. Gaillard, E. Villemain, D. Rigaud, M. Valenza, M. Rolland, S. Gaillard, E. Villemain, D. Rigaud, M.V. Low, and H.A.L. Id, 3, 1825 (1993). E. Villemain, S. Gaillard, M. Rolland, and A. Joullie, 20, 162 (1993).
 A. Vogt, H. Hartnagel, G. Miehe, H. Fuess, and J. Schmitz, J. Vac. Sci. Technol. B 14, 3514 (1996). A. Vogt, A. Simon, and H.L. Hartnagel, J. APplieds Phys. 83, (1998).
 J. Sigmund, M. Saglam, A. Vogt, H.L. Hartnagel, and V. Buschmann, 228, 625 (2001). ⁷⁹ K. Varblianska, K. Tzenev, and T. Kotsinov, Phys. STATUS SOLIDI A-APPLIED Res. 163, 387

L.B. Karlina, A.S. Vlasov, M.M. Kulagina, and N.K. Timoshina, 40, 346 (2005).
 A.W. Bett and O.V. Sulima, Semicond. Sci. Technol. 18, S184 (2003).
 M.K. Hudait, M. Brenner, and S. a. Ringel, Solid. State. Electron. 53, 102 (2009).

- A. Piotrowska, T. Piotrowski, S. Kasjaniuk, M. Guziewicz, S. Gierlotka, X.W. Lin, M.S. Division, and S. Kwiatkowski, 87, 419 (1995).
 S.A.A.B.K.K.S. Priyabadini and M. Amann, 259 (2009).
 C. Lauer, O. Dier, and M. Amann, (2006).
 R.K. Huang, C.A. Wang, C.T. Harris, M.K. Connors, and D.A. Shiau, 33, (2004).
 N.A. Pfiester and T.E. Vandervelde, Phys. Status Solidi Appl. Mater. Sci. 214, (2017).
 C. Shemelya, D. Demeo, N.P. Latham, X. Wu, C. Bingham, W. Padilla, and T.E. Vandervelde, Appl. Phys. Lett. 104, (2014).